Integrated Electrokinetic Sample Focusing and Surface Plasmon Resonance Imaging System for Measuring Biomolecular Interactions

ARTICLE *in* ANALYTICAL CHEMISTRY · MARCH 2009

Impact Factor: 5.64 · DOI: 10.1021/ac802668z · Source: PubMed

5 AUTHORS, INCLUDING:

Edwin T Carlen
University of Tsukuba
72 PUBLICATIONS **755** CITATIONS
SEE PROFILE

Dietrich Kohlheyer
Forschungszentrum Jülich
47 PUBLICATIONS **620** CITATIONS
SEE PROFILE

Richard B M Schasfoort
University of Twente
104 PUBLICATIONS **2,446** CITATIONS
SEE PROFILE

Albert Van den Berg
University of Twente
675 PUBLICATIONS **12,088** CITATIONS
SEE PROFILE

Article

Integrated Electrokinetic Sample Focusing and Surface Plasmon Resonance Imaging System for Measuring Biomolecular Interactions

Ganeshram Krishnamoorthy, Edwin T. Carlen, Dietrich Kohlheyer, Richard B. M. Schasfoort, and Albert van den Berg

Anal. Chem., **2009**, 81 (5), 1957-1963• DOI: 10.1021/ac802668z • Publication Date (Web): 02 February 2009

Anal. Chem. **2009,** *81,* 1957–1963

Integrated Electrokinetic Sample Focusing and Surface Plasmon Resonance Imaging System for Measuring Biomolecular Interactions

Ganeshram Krishnamoorthy,* Edwin T. Carlen, Dietrich Kohlheyer, Richard B. M. Schasfoort, and Albert van den Berg

BIOS Lab-On-A-Chip Group, MESA+ Institute for Nanotechnology, University of Twente, P.O. Box 217, 7500 AE Enschede, The Netherlands

Label-free biomolecular binding measurement methods, such as surface plasmon resonance (SPR), are becoming increasingly more important for the estimation of real-time binding kinetics. Recent advances in surface plasmon resonance imaging (iSPR) are emerging for label-free microarray-based assay applications, where multiple biomolecular interactions can be measured simultaneously. However, conventional iSPR microarray systems rely on protein printing techniques for ligand immobilization to the gold imaging surface and external pumps for analyte transport. In this article, we present an integrated microfluidics and iSPR platform that uses only electrokinetic transport and guiding of ligands and analytes and, therefore, requires only electrical inputs for sample transport. An important advantage of this new approach, compared to conventional systems, is the ability to direct a single analyte to a specific ligand location in the microarray, which can facilitate analysis parallelization. Additionally, this simple approach does not require complicated microfluidic channel arrangements, external pumps, or valves. As a demonstration, kinetics and affinity have been extracted from measured binding responses of human IgG and goat antihuman IgG using a simple 1:1 model and compared to responses measured with conventional pressure driven analyte transport. The measured results indicate similar binding kinetics and affinity between the electrokinetic and pressure-driven sample manipulation methods and no cross contamination to adjacent measurement locations has been observed.

Surface plasmon resonance (SPR) and surface plasmon resonance imaging (iSPR)[1] are rapidly developing instruments for monitoring biomolecular interactions in the fields of genomics,[2,3] proteomics,[4,5] and cellomics,[6,7] where affinity and binding kinetics can be estimated directly from their measured responses.[8] The combination of SPR with microfluidics, or lab-on-a-chip (LOC) technology, is particularly compelling for bioanlytical systems[9,10] because the two techniques can be integrated relatively easily and has the potential for fast and automated biomolecular analysis systems with ultrasmall sample volumes.[11]

Integrated SPR-LOC systems are not new.[12] Commercially available SPR systems, such as the Biacore (GE Healthcare)[13] and ProteOn (Bio-Rad Laboratories)[14] instruments use LOC flow cells for fluid transport to their SPR systems. Additionally, there are many recent reports describing new trends and designs for integrated SPR-LOC based measurement systems[15−19] and many reports of applications for integrated LOC-SPR systems, such as, immunoassays,[20] protein−aptamer interactions,[21] and cellular detection.[22] Although significant progress has been made over the last several years, more development is needed to further automate and simplify SPR-LOC systems. Additionally, the amount of sample required for diagnostic purposes can be further reduced by adopting ligand microarray formats on the SPR imaging surface, which will facilitate multianalyte iSPR assays.[23] Integrating LOC technology to microarray based detection techniques has

* To whom correspondence should be addressed. Phone: 0031-53-4892724. Fax: 0031-53-4893595. E-mail: g.krishnamoorthy@tnw.utwente.nl.

(1) Piscevic, D.; Knoll, W.; Tarlov, M. J. *Supramol. Sci.* **1995**, *2*, 99–106.
(2) Baldrich, E.; Restrepo, A.; O'Sullivan, C. K. *Anal. Chem.* **2004**, *76*, 7053–7063.
(3) Ehlers, I.; Horke, S.; Reumann, K.; Rang, A.; Grosse, F.; Will, H.; Heise, T. *J. Biol. Chem.* **2004**, *279*, 43437–43447.
(4) Ikeda, Y.; Imai, Y.; Kumagai, H.; Nosaka, T. *Proc. Natl. Acad. Sci. U.S.A.* **2004**, *101*, 10732–10737.
(5) Yamaguchi, S.; Mannen, T.; Nagamune, T. *Biotechnol. Lett.* **2004**, *26*, 1081–1086.
(6) Sadamoto, R.; Niikura, K.; Ueda, T.; Monde, K.; Fukuhara, N.; Nishimura, S.-I. *J. Am. Chem. Soc.* **2004**, *126*, 3755–3761.
(7) Verdonck, F.; Cox, E.; Vancaeneghem, S.; Goddeeris, B. M. *FEMS Immunol. Med. Microbiol.* **2004**, *41*, 243–248.
(8) Doyle, M. L.; Myszka, D. G.; Chaiken, I. M. *J. Mol. Recognit.* **1996**, *9*, 65–74.
(9) Brockman, J. M.; Frutos, A. G.; Corn, R. M. *J. Am. Chem. Soc.* **1999**, *121*, 8044–8051.
(10) Lee, H. J.; Goodrich, T. T.; Corn, R. M. *Anal. Chem.* **2001**, *73*, 5525–5531.
(11) Lew, H. S.; Fung, Y. C. *J. Biomech.* **1969**, *2*, 105–119.
(12) Sjoelander, S.; Urbaniczky, C. *Anal. Chem.* **1991**, *63*, 2338–2345.
(13) Morton, T. A.; Myszka, D. G.; Chaiken, I. M. *Anal. Biochem.* **1995**, *227*, 176–185.
(14) Bravman, T.; Bronner, V.; Lavie, K.; Notcovich, A.; Papalia, G. A.; Myszka, D. G. *Anal. Biochem.* **2006**, *358*, 281–288.
(15) Figeys, D.; Pinto, D. *Electrophoresis* **2001**, *22*, 208–216.
(16) Schasfoort, R. B. M. *Expert Rev. Proteomics* **2004**, *1*, 123–132.
(17) Gervais, T.; Jensen, K. F. *Chem. Eng. Sci.* **2006**, *61*, 1102–1121.
(18) Galopin, E.; Beaugeois, M.; Pinchemel, B.; Camart, J. C.; Bouazaoui, M.; Thomy, V. *Biosens. Bioelectron.* **2007**, *23*, 746–750.
(19) Skottrup, P. D.; Nicolaisen, M.; Justesen, A. F. *Biosens. Bioelectron.* **2008**, *24*, 339–348.
(20) Luo, Y.; Yu, F.; Zare, R. N. *Lab Chip* **2008**, *8*, 694–700.
(21) Wang, Z.; Wilkop, T.; Xu, D.; Dong, Y.; Ma, G.; Cheng, Q. *Anal. Bioanal. Chem.* **2007**, *389*, 819–825.
(22) Lei, K. F.; Law, W. C.; Suen, Y. K.; Li, W. J.; Ho, H. P.; Lin, C.; Kong, S. K. *Proc. 5th IEEE Conf. Nanotechnol.* **2005**, *1*, 515–518.
(23) MacBeath, G.; Schreiber, S. L. *Science* **2000**, *289*, 1760–1763.

10.1021/ac802668z CCC: $40.75
Published on Web 02/02/2009

been previously described[24,25] and is currently an active area of research.[26−29] Commercial systems, such as Biacore's Flexchip[30] and the IBIS-iSPR (IBIS Technologies, b.v. Hengelo, The Netherlands)[31,32] use a microarray approach together with an iSPR-LOC system. One of the major advantages of these new systems is that they are completely automated. However, the conventional systems use syringe pumps for sample transport, which requires a complex matrix of valves and connectors for multiple analyte analysis and it is not currently possible to guide a single analyte to a single ligand location. One way to achieve this is to use a combination of electro-osmotic flow (EOF)[33−35] for sample transport and electrokinetic focusing (EKF)[36−42] for sample guiding to specific array locations, which may be important for instrument miniaturization and scaling to larger numbers of the samples where conventional techniques will no longer be possible.

In this paper, we present a simple technique to combine EOF, for in situ ligand immobilization and sample transport, and EKF, for sample guiding, in a LOC simultaneously with iSPR for biomolecular interaction measurements in a microarray format with multiple sites and all electrical control. For demonstration purposes, we use a single ligand type immobilized on various locations of an array with 24 gold imaging sites (6 × 4 array) and a single sample is focused to each row and the subsequent real-time biomolecular interactions have been measured. We first demonstrate EKF with a sample (3% glycerol in 5 mM HEPES buffer and rhodamine B) focused to various locations of the chip using predetermined guiding voltages. Fluorescence microscopy images of the focused flow at each location were captured in order to clearly identify the flow profile. Subsequently, the SPR signal changes were measured during sample focusing. Finally, combined EKF and iSPR is demonstrated by measuring biomolecular interactions of human IgG and goat antihuman IgG during sample focusing, and results are presented and compared to iSPR measurement results with conventional pressure driven sample transport.

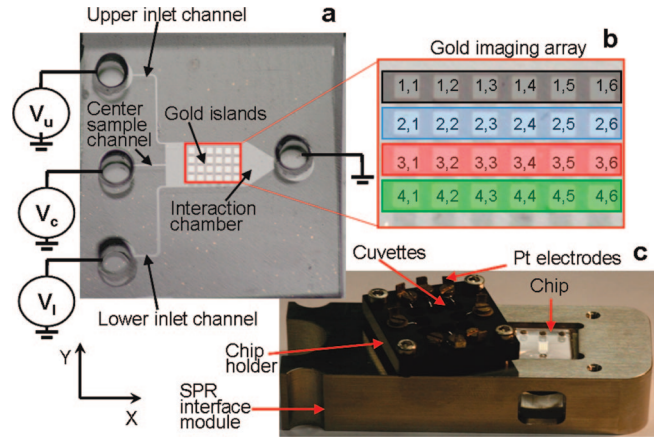

Figure 1. (a) Microfabricated chip with electric circuit representation; (b) iSPR gold imaging array with location (row, column); (c) iSPR chip interface module comprised of SPR slider for hemispherical prism and chip with chip holder inserted with platinum electrodes for high voltage electric power supply.

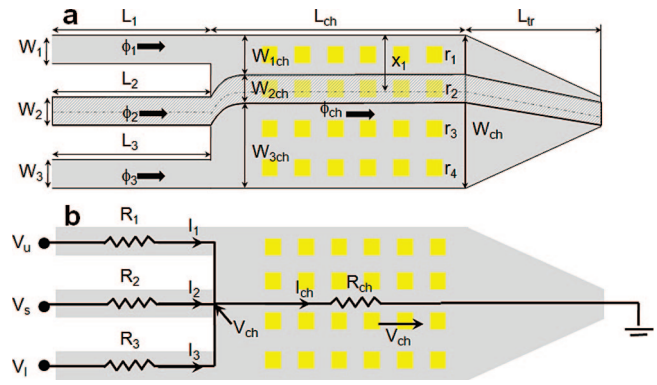

Figure 2. (a) Schematic illustration of the EKF chip and corresponding parameters. Example shows EKF to row 2. Here, r_1, r_2, r_3, and r_4 represents row 1 through row 4, respectively. The microchannel widths are W_1, W_2, and W_3, and the reaction chamber width is W_{ch}. W_{1ch}, W_{2ch}, and W_{3ch} is the width of the top guiding stream, sample stream, and bottom guiding stream, respectively. ϕ_1, ϕ_2, ϕ_3, and ϕ_{ch} represent the flux in channel 1, channel 2, channel 3, and the reaction chamber, respectively. L_1, L_2, L_3, L_{ch}, and L_{tr} are the length of channel 1, channel 2, channel 3, the rectangular chamber, and the trapezoid, respectively. x_1 is the distance from the top of the chip to the center of the sample stream. (b) Electrical circuit representation of the electrokinetic focusing chip. R_1, R_2, R_3, and R_{ch} represent the resistors in the corresponding channel and reaction chamber. I_1, I_2, I_3, and I_{ch} is the current in the corresponding channels and chamber. V_u, V_c, V_l, and V_{ch} represents the voltage in the upper channel (channel 1), sample channel (channel 2), lower channel (channel 3), and chamber, respectively.

MATERIALS AND METHODS

Microfabrication. The microfluidic biochip (size, 15 × 15 mm^2) presented here has two layers. The top PDMS layer includes channel structures, interaction chamber, and reservoir holes for sample introduction and electrode interfacing. The

(24) Figeys, D. *Proteomics* **2002**, *2*, 373–382.
(25) Situma, C.; Hashimoto, M.; Soper, S. A. *Biomol. Eng.* **2006**, *23*, 213–231.
(26) Lee, K. H.; Su, Y. D.; Chen, S. J.; Tseng, F. G.; Lee, G. B. *Biosens. Bioelectron.* **2007**, *23*, 466–472.
(27) Mauriz, E.; Calle, A.; Manclus, J. J.; Montoya, A.; Escuela, A. M.; Sendra, J. R.; Lechunga, L. M. *Sens. Actuators, B* **2006**, *118*, 399–407.
(28) Yuk, J. S.; Kim, H. S.; Jung, J. W.; Jung, S. H.; Lee, S. J.; Kim, W. J.; Han, J. A.; Kim, Y. M.; Ha, K. S. *Biosens. Bioelectron.* **2006**, *21*, 1521–1528.
(29) Homola, J.; Vaisocherová, H.; Dostálek, J.; Piliarik, M. *Methods* **2005**, *37*, 26–36.
(30) Rich, R. L.; Cannon, M. J.; Jenkins, J.; Pandian, P.; Sundaram, S.; Magyar, R.; Brockman, J.; Lambert, J.; Myszka, D. G. *Anal. Biochem.* **2008**, *373*, 112–120.
(31) Lokate, A. M. C.; Beusink, J. B.; Besselink, G. A. J.; Pruijn, G. J. M.; Schasfoort, R. B. M. *J. Am. Chem. Soc.* **2007**, *129*, 14013–14018.
(32) Beusink, J. B.; Lokate, A. M. C.; Besselink, G. A. J.; Pruijn, G. J. M.; Schasfoort, R. B. M. *Biosens. Bioelectron.* **2008**, *23*, 839–844.
(33) Ellender, R. D.; Morton, F.; Whelan, J.; Sweet, B. H. *Prep. Biochem.* **1972**, *2*, 215–228.
(34) Gao, Y.; Lin, F. Y. H.; Hu, G.; Sherman, P. M.; Li, D. *Anal. Chim. Acta* **2005**, *543*, 109–116.
(35) Hu, G.; Gao, Y.; Sherman, P. M.; Li, D. *Microfluid. Nanofluid.* **2005**, *1*, 346–355.
(36) Fu, L. M.; Yang, R. J.; Lee, G. B.; Liu, H. H. *Anal. Chem.* **2002**, *74*, 5084–5091.
(37) Fu, L. M.; Yang, R. J.; Lee, G. B. *Anal. Chem.* **2003**, *75*, 1905–1910.
(38) Besselink, G. A. J.; Vulto, P.; Lammertink, R. G. H.; Schlautmann, S.; van den Berg, A.; Olthuis, W.; Engbers, G. H. M.; Schasfoort, R. B. M. *Electrophoresis* **2004**, *25*, 3705–3711.
(39) Kohlheyer, D.; Besselink, G. A. J.; Lammertink, R. G. H.; Schlautmann, S.; Unnikrishnan, S.; Schasfoort, R. B. M. *Microfluid. Nanofluid.* **2005**, *1*, 242–248.
(40) Wu, C. H.; Yang, R. J. *Electrophoresis* **2006**, *27*, 4970–4981.
(41) Kohlheyer, D.; Unnikrishnan, S.; Besselink, G. A. J.; Schlautmann, S.; Schasfoort, R. B. M. *Microfluid. Nanofluid.* **2007**, *4*, 557–564.
(42) Pan, Y. J.; Ren, C. M.; Yang, R. J. *J. Micromech. Microeng.* **2007**, *17*, 820–827.

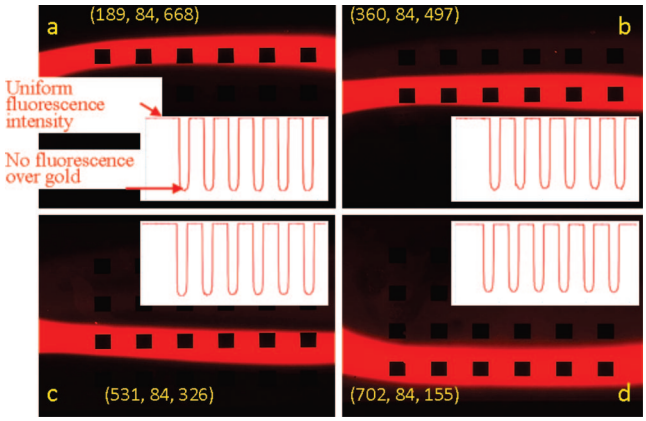

Figure 3. Fluorescence microscopy images demonstrating sample stream focusing (3% glycerol in 5 mM HEPES + rhodamine B over the six gold islands in each row (a–d). Inset plot shows the uniform intensity profile of the focused sample stream. No fluorescence over gold islands was visible due to the observation from the bottom of the chip.

Table 1. Calculated Voltages Required to Focus to Various Rows of Gold Islands by Keeping the Flow Speed of 300 μm/s and Sample Stream Width of 300 μm

rows	V_u (V)	V_c (V)	V_l (V)
1	189	84	668
2	360	84	497
3	531	84	326
4	702	84	155

PDMS mold was prepared in a cleanroom using a standard procedure.[43] The reservoir holes were manually punched with a sharp hollow tube. The bottom glass layer, refractive index matched (n = 1.52) to the hemispherical prism of the iSPR instrument (IBIS Technologies b.v., Hengelo, The Netherlands), has patterned gold islands for SPR imaging. The gold iSPR islands were electron beam evaporated externally (sSens b.v. Hengelo, The Netherlands) and patterned on the glass layer. Following, gold island patterning, the glass chips were coated with derivatized hydrogel preactivated for covalent immobilization (XanTec GmbH, Muenster, Germany). The PDMS chips were ultrasonically cleaned in isopropanol for 15 min prior to any further processing and subsequently dried with dry nitrogen and cleaned with oxygen plasma for 5 min. A thin glue (Norland Optical Adhesive 81, Norland) was spin coated on a blank wafer at 8000 rpm for 60 s, which is used as the blotter for the stamp-and-stick bonding technique.[44] The molded PDMS layers were carefully pressed into the glue blotter layer, removed, and subsequently bonded to the glass chip. The bonded stack was then cured in UV light (λ = 359 nm) for 45 min. The final chip is shown in Figure 1a. The patterned square gold islands are 200 μm on a side and the pitch (center to center distance) is 500 μm. The thickness of the gold imaging layer is 47 nm. The thickness of the bottom glass layer is 1.1 mm and the PDMS layer is 2 mm. Each reservoir hole is 2 mm in diameter, and the depth of the microchannel and interaction chamber is 35 μm. The interaction chamber has width W_{ch} = 2.5 mm and length L_{ch} = 4.5 mm (Figure 2).

Electrokinetic Focusing. The main goal of using EKF is to focus the sample stream over various rows of gold islands immobilized with ligands and to simultaneously measure the biomolecular interaction using an iSPR system. EKF in a microfluidic chip was described in detail elsewhere[38] and later reported for controlling the flow in a microreactor.[39] In brief, EKF is a valveless and pumpless method for controlling the sample stream profile in a laminar flow chamber. A schematic illustration of EKF is shown in Figure 2a, where the sample from the center inlet is focused to the second row r_2 of the gold island imaging array. An equivalent electrical circuit is shown in Figure 2b where resistances R_i are determined by sample conductivity and channel dimensions. By alteration of the control voltages (V_u, upper channel voltage; V_l, lower channel voltage), the sample stream can be directed to each of the imaging array rows r_i. The sample flow is controlled by the center voltage (V_c, sample voltage), which also controls the flow velocity and sample stream width according to the distance x_1, shown in Figure 2b. The chip was placed in a SPR slider (Figure 1c) and clamped with the custom chip holder, which includes platinum electrodes that are connected to a computer controlled power supply (IBIS 411, IBIS Technologies b.v., Hengelo, The Netherlands). The upper and lower reservoirs were filled with 5 mM HEPES buffer, and the center reservoir is filled with the sample. The outlet reservoir voltage was set to ground, and the voltages for the guiding streams, as well as sample streams, were individually controlled. Electro-osmotic mobility is assumed to be constant $\mu_{EOF} \approx 5 \times 10^{-8}$ m^2/V s.[39] The guiding stream and sample transport voltages are calculated using $V_i = (\Phi_i L_i / A_i \mu_{EOFi}) + (R_{ch}/\mu_{EOFi}) \Sigma(\Phi_j L_j / R_j A_j)$, where A_i and A_j (m^2) are the cross-sectional areas of the channels and chamber, Φ_i and Φ_j are the flow fluxes (m^3/min), and R_{ch} and R_j are the electrical resistances (Ω) of the channels and chamber, respectively. A detailed derivation and explanation of the equation was previously discussed.[39] The calculated guiding voltages are summarized in Table 1. Some parts of the experiment use electro-osmotic flow (EOF) to transport the buffer to the various location of the chip, which is done with constant voltages (V_a and V_b) applied to the upper and lower reservoirs. Rhodamine B was added to the sample solution (3% glycerol in 5 mM HEPES) for flow profile visualization, and images were recorded with an inverted fluorescence microscope (Olympus IX51) color CCD imaging camera.

Surface Plasmon Resonance. The angle scanning iSPR system (IBIS-iSPR, IBIS Technologies b.v., Hengelo, The Netherlands) used for experiments has been described previously.[31,32] In brief, the gold islands of the microarray are exposed to polarized light at a certain controlled incident angle. The refractive index change is proportional to the amount of adsorption or binding at the surface, which results in a measurable shift of the surface plasmon resonance condition, called the resonant angle. The measured response is converted to the time domain, which is referred to as a sensorgram. There are three main measurement phases of the sensorgram: baseline phase, a running buffer in contact with the sensor surface to establish the baseline

(43) Linder, V.; Verpoorte, E.; Thormann, W.; de Rooij, N. F.; Sigrist, H. *Anal. Chem.* **2001**, *73*, 4181–4189.
(44) Schlautmann, S.; Besselink, G. A. J.; Radhakrishna Prabhu, G.; Schasfoort, R. B. M. *J. Micromech. Microeng.* **2003**, *13*, S81–Ss84.

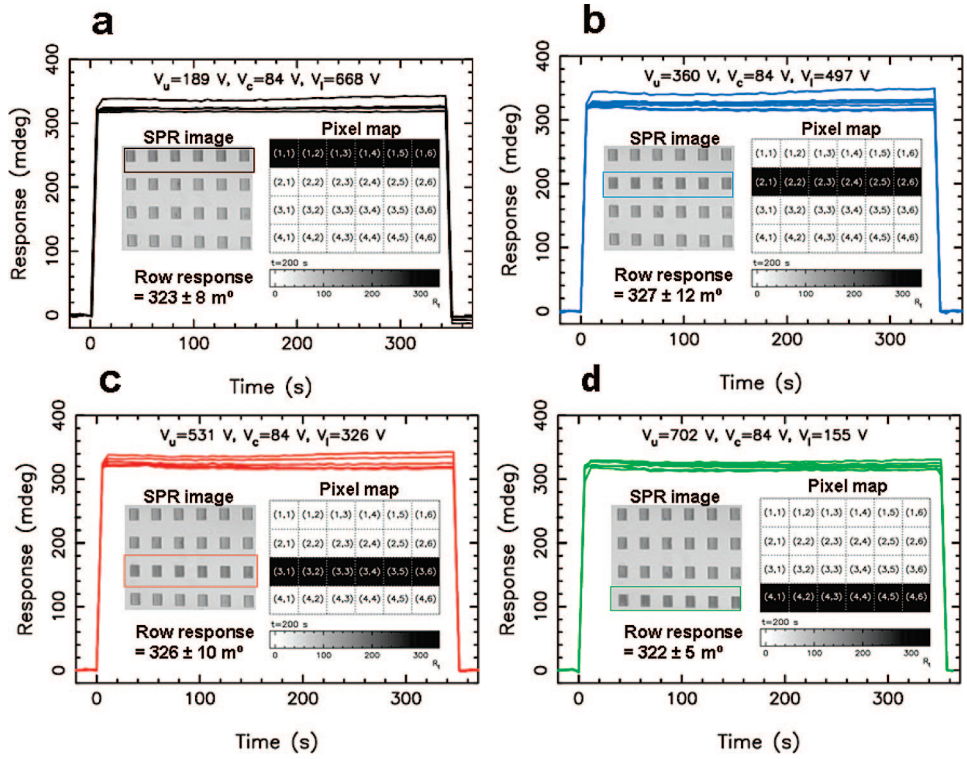

Figure 4. iSPR measurements of 3% glycerol in 5 mM HEPES focused at each row (columns shown with different colors) (a) row 1, (b) row 2, (c) row 3, (d) row 4. Inset image obtained from SPR CCD camera while focusing was done to those rows. Clear color distinction was observed between the focused and nonfocused rows. A grayscale pixel map of each row is also shown. Electrical focusing voltages are shown as V_u, V_c, and V_l.

responses; association phase, sample containing the target analyte [A] is injected to the interaction chamber and the ligands [B] immobilized on the surface, the capturing element on the sensor surface binds to the target resulting in complex formation [AB]; and dissociation phase, injection of running buffer again which leads to dissociation of bound molecules from the surface. The EKF chip was placed on the hemispherical prism, separated by a droplet of refractive index matching oil, which is integrated in the SPR slider (Figure 1c).

The SPR responses as well as real time images were recorded during EKF to each row using a solution of 3% glycerol in 5 mM HEPES buffer. Biomolecular interaction experiments of human IgG−goat antihuman IgG were also performed using the EKF technique. A solution of 500 μg/mL human IgG (Sigma, The Netherlands) was immobilized on the gold islands using an EOF ($V_a = V_u = V_l = 200$ V dc) transport. The remaining active sites were blocked with 1 M ethanolamine (Sigma, The Netherlands) for 1 h and subsequently washed. A baseline measurement was done using a 5 mM HEPES buffer. An analyte solution of 133 nM goat antihuman IgG (Molecular Probes) was focused to the first row for 300 s followed by a dissociation phase with a running buffer over the gold islands for 300 s ($V_b = V_u = V_l = 200$ V). This procedure was repeated for the various rows of the array. The measured sensorgrams were fitted to a 1:1 interaction model[13] using the commercially available software (Scrubber, Biologics Inc., Australia). The results are discussed in detail in the next section.

RESULTS AND DISCUSSION

Electrokinetic Flow Profiling. Fluorescence microscopy images of 3% glycerol/rhodamine B focused to each row of the array is shown in Figure 3a−d, clearly showing the flow profile. The measured fluorescence intensity profiles are shown in the insets of Figure 3a−d, which show uniform sample concentrations along each row of the imaging islands. The dark regions are caused by the gold islands blocking light from the inverted microscope. Low flow rates can be affected by sample diffusion, and therefore, proper flow velocity (~300 μm/s) has to be considered for measurements. Following sample focusing to different rows, we have observed a small amount of fluorescence remaining in the previous row. We assume this is due to rhodamine adsorption to the PDMS surface, but further investigation is required to verify the cause. However, the SPR images do not indicate any sample crossover to adjacent rows.

The chip alignment of the reaction chamber to the gold-island imaging array is very important and unsymmetrical alignment results in unsymmetric focusing voltages. Additionally, the distance from the sample inlet to rows r_1 and r_4 is larger than the distance to rows r_2 and r_3 and, therefore, requires higher focusing voltages. Finally, the voltage drop across the gold imaging array may lead to electrochemical reactions, as previously reported,[45−47] when the gold layer is exposed to high voltages for long times. A low conductivity (5 mM HEPES, $\sigma \approx$ 127 μS/cm) buffer is used to minimize voltage drops across the gold islands in the interaction chamber, which significantly reduces degradation of gold imaging islands.

Integrated EKF-SPR: Glycerol. The combination of EKF and SPR imaging has been demonstrated by EKF of a 3% glycerol sample to each array row and simultaneous SPR measurement at

(45) Abelès, F.; Lopez-Rios, T. *Solid State Commun.* **1975**, *16*, 843–847.
(46) Gordon, J. G., II; Ernst, S. *Surf. Sci.* **1980**, *101*, 499–506.
(47) Kolb, D. M. *Prog. Surf. Sci.* **1996**, *51*, 109–173.

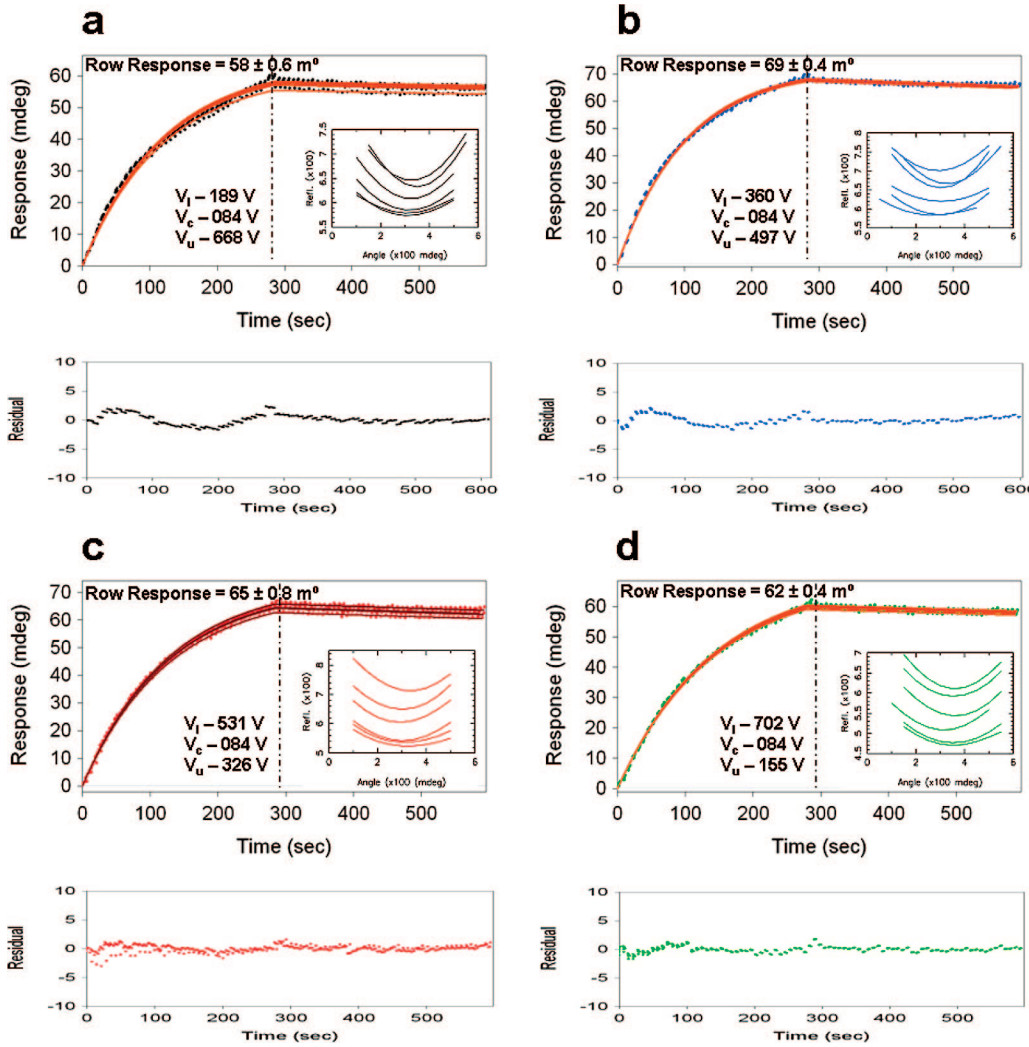

Figure 5. Raw sensorgrams (a−d) of each row of human IgG (500 μg/mL)−antihuman IgG (133 nM) interaction using electrokinetic focusing. Human IgG covalently immobilized on gold/hydrogel surface using 200 V EOF. It also shows the uniformity of the response observed with very little standard deviation. Insets: SPR dips of each gold islands (ROIs). Kinetics and affinity calculated from the 1:1 interaction model (global analysis) fit using Scrubber software. Fit results are represented by the orange curve, and the resultant values are shown in Table 2. Fitting residual plots for each row are shown with their respective colors.

Table 2. Extracted 1:1 Model Parameters[a]

rows	response (mdeg)	std deviation (mdeg)	$k_a \times 10^4$ (M^{-1} s^{-1})	$k_d \times 10^{-5}$ (s^{-1})	K_D (nM)	R_{max}
1	58	0.60	6.18 ± 0.01	9.27 ± 1.54	1.50 ± 0.25	64 ± 0.88
2	69	0.38	7.39 ± 0.05	8.61 ± 0.32	1.16 ± 0.04	72 ± 0.43
3	65	0.83	5.84 ± 0.25	11.3 ± 1.46	1.99 ± 0.23	73 ± 1.96
4	62	0.39	5.24 ± 0.09	10.4 ± 0.87	1.97 ± 0.19	71 ± 0.40

[a] Association rate (k_a), dissociation rate (k_d), and affinity constant (K_D) from experimental data for each row using electrokinetic focusing. Total number of measurement sites in each row is 6.

each gold island in the row, as shown in Figure 4a−d. The gold islands with EK focused glycerol sample shows the shifted resonant angle with respect to the buffer clearly showing the combination of EKF with SPR imaging. The left inset of Figure 4a−d shows a captured SPR image of the surface using a CCD camera integrated with the iSPR system while focusing to the respective rows. The gold islands of the focused row clearly become a darker color. The right insets in Figure 4 show grayscale pixel maps of the measured SPR response in each row. There are 24 pixels in the image map, separated by dotted lines, corresponding to the 24 imaging islands, and the grayscale color of each pixel represents the measured response of each imaging island at time $t = 200$ s. The lower scale bar in each case shows how the grayscale varies from $R_t = 0$ to $R_t = 340$ mdeg. As can be seen from each pixel map, the measured response of the focused row is ~300× higher than the neighboring rows indicating minimal sample cross-over and very uniform measured response across the row.

Integrated EKF-SPR: Biomolecular Interaction. Biomolecular interaction measurements in combination with sample focusing were conducted. First, 500 μg/mL of human IgG ligand was introduced to the interaction chamber with EOF ($V_c = 200$

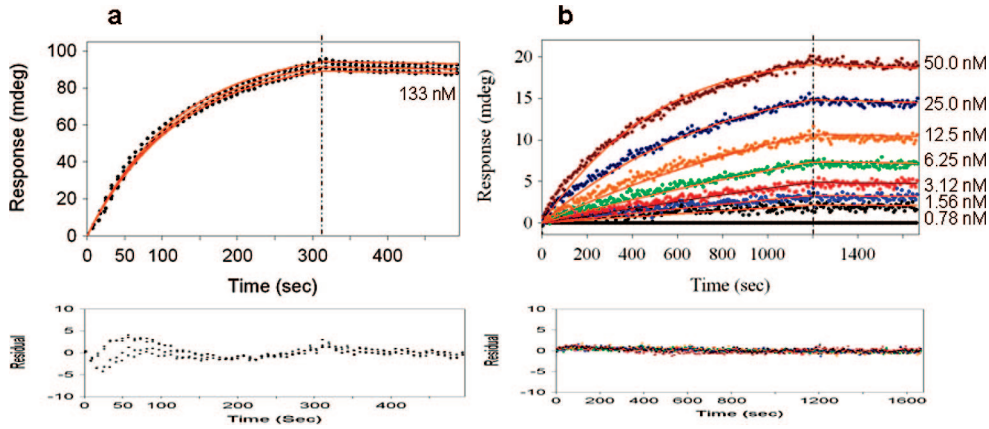

Figure 6. (a) Sensorgrams of the four spots having the same concentrations obtained by the injection of analyte solution (133 nM) on a hydrogel/gold surface. (b) Sensorgram of human IgG immobilization on a hydrogel/gold surface (500 μg/mL) and various goat antihuman IgG concentrations (50, 25, 12.5, 6.25, 3.125, 1.5625, and 0.78 nM). Fit results are represented by the orange curve, and the resultant values are shown in Table 3.

Table 3. Comparison of Extracted 1:1 Interaction Model Parameters from Three Different Measurement Approaches: Conventional, Pressure Driven, and Electrokinetic Focusing Experiments[a]

no.	approach	$k_a \times 10^4$ (M^{-1} s^{-1})	$k_d \times 10^{-5}$ (s^{-1})	K_D (nM)
1	electrokinetic focusing	6.17 ± 0.10	9.88 ± 0.56	1.66 ± 0.35
2	pressure driven flow	5.95	6.64	1.11
3	conventional kinetics	4.91	4.96	1.01

[a] Conventional (7 different analyte concentrations), pressure driven (4 different measurement sites), and electrokinetic focusing experiments (24 measurement sites that is 6 from each row).

V), which is covalently immobilized on the hydrogel coated gold islands. Human IgG was introduced to the interaction chamber through the center inlet only, and therefore, a long time was required to uniformly adsorb the ligand on the gold islands. A low voltage is required to prevent damaging the gold islands.[48,49] Unbound ligands were removed from the surface by electrically washing with 5 mM HEPES buffer and applying 200 V to both of the buffer inlets V_u and V_l. During the surface washing step, the gold islands were SPR imaged and the sample focusing was conducted after a steady baseline signal was achieved. The results of the focusing experiments are shown in Figure 5a–d. The measured responses are proportional to immobilized ligand density (not shown). Before the sample stream is focused to the next row, the flow is stopped and buffer was injected through the chip with an applied voltage of 200 V to the buffer reservoirs. The dissociation profile was measured in each case. For example, when the sample was focused to row 2, the dissociation profile of row 1 was measured continuously since the guiding stream consists of a buffer suitable for dissociation (not shown). We have not observed any cross-reaction with other rows while performing the focusing experiment. A problem encountered while performing the biomolecular measurements was a reduction in flowrate with increased time, which is attributed to protein adsorption to the PDMS channel walls. By careful control of the protein concentration and experiment time, the effects of protein adsorption to PDMS can be significantly reduced. This problem can be addressed by using a surface treatment to reduced protein adsorption to PDMS[50] or by using a different channel material. Presently, regeneration steps have not been developed for this system.

The raw sensorgram data were fitted to a 1:1 simple interaction model, and the results are shown as orange overlay plots in Figure 5a–d. The 1:1 interaction model is used in this case for comparing the different sample transport methods only and not a rigorous kinetics evaluation, which is beyond the scope of this article. Since it is well-known that the analyte goat antihuman IgG used in this work is bivalent in nature, a 1:1 interaction model is not appropriate for a meaningful kinetics evaluation. The maximum measurement response R_{max} extrapolated from the sensorgram data was kept local to each measurement sites, whereas association and dissociation rates were kept global for parameter extraction and fitting.[14] The data analysis results in single association and dissociation rates and, therefore, a single affinity constant representing the interactant pair binding. Since the concentration of the analyte and ligands are approximately uniform, the extracted kinetics and affinity should be in the same order of magnitude for various rows. The extracted parameters are shown in Table 2. The affinity constant K_D extracted for all the four rows is of same order of magnitude even though the values are different due to differences in ligand densities, which can be solved by optimizing the immobilization procedure. The possible sources of error include the iSPR system, heterogeneity in analytes, gold surface homogeneity, and rebinding effects. In practice, the analyte concentration should be considered in the same range as the affinity constants in order to predict accurate kinetic parameters. The analyte concentration used in these experiments is larger than the extracted affinity constant; however, this does not affect the demonstration of combined EKF sample focusing and iSPR. The SPR dips shown in the insets of Figure 5a–d show that the SPR minimum varies between the gold islands. Since the data measured during the baseline is zeroed, it is assumed that the effect of EKF is negligible and does not show any significant difference during the EKF. The average and standard deviation

(48) Genshaw, M. A.; Damjanovic, A.; Bockris, J. O'M. *J. Electroanal. Chem.* **1967**, *15*, 163–172.
(49) Damjanovic, A.; Genshaw, M. A.; Bockris, J. O'M. *J. Electroanal. Chem.* **1967**, *15*, 173–180.

Table 4. Analysis of the Fitting Residuals from Scrubber for All 24 Imaging Islands[a]

	spot 1	spot 2	spot 3	spot 4	spot 5	spot 6
			Association Phase (mdeg)			
row 1	0.03 ± 1.14	0.02 ± 1.14	0.07 ± 1.14	−0.01 ± 1.15	0.01 ± 1.14	0.12 ± 1.18
row 2	−0.04 ± 0.97	−0.02 ± 0.95	0.05 ± 0.98	0.08 ± 0.98	0.10 ± 0.99	0.07 ± 0.98
row 3	0.15 ± 0.55	0.20 ± 0.55	0.11 ± 0.51	−0.77 ± 0.80	0.22 ± 0.55	0.01 ± 0.55
row 4	0.08 ± 0.60	−0.05 ± 0.62	−0.17 ± 0.66	−0.10 ± 0.63	0.02 ± 0.61	−0.03 ± 0.61
			Dissociation Phase (mdeg)			
row 1	0.03 ± 0.37	0.04 ± 0.36	0.01 ± 0.37	0.06 ± 0.36	0.04 ± 0.36	−0.05 ± 0.38
row 2	0.09 ± 0.38	0.07 ± 0.37	0.04 ± 0.38	0.02 ± 0.36	0.01 ± 0.36	0.03 ± 0.37
row 3	0.01 ± 0.37	−0.01 ± 0.38	−0.01 ± 0.40	0.39 ± 0.38	−0.02 ± 0.37	0.07 ± 0.36
row 4	0.01 ± 0.40	0.06 ± 0.40	0.10 ± 0.406	0.10 ± 0.40	0.04 ± 0.40	0.07 ± 0.40

[a] For each island, the mean and standard deviation are calculated over the time duration of the measurement phase. The assocation and dissociation phases are each 300 s in duration. The statistical distribution was graphically estimated with histograms and fit to a Gaussian distribution model (data not shown). Approximately 50 data points were considered in each association phase, and dissociation residual values were obtained from the fit.

of the response and extracted parameters were obtained from six measurement sites called "region of interests" (ROI) from a single array row. The standard deviations of the estimated affinity constants from the six ROIs are shown in Table 2. The fitting residuals are shown in Figure 5a−d. Table 4 shows the mean and standard deviation for each gold island during the association and dissociation phases, which was calculated from the residuals obtained from the fitting of the raw data to a 1:1 model assuming a Gaussian distribution (histograms not shown). The assocation and dissociation phases are each 300 s in duration.

Additional experiments have been performed and compared to the EKF-SPR results. First, the human IgG−antihuman IgG interactant pair was investigated with the same analyte concentration on a commercially available hydrogel coated gold sensor disk (HCX 80m from XanTec GmbH, Muenster, Germany) with conventional pressure driven flow. The sensorgrams, fits, and residual plots are shown in Figure 6a. There is a small response variation (∼1.5%) between different ROIs in a single row; however, these variations are not caused by EKF as similar results were obtained from experiments done using conventional pressure driven flow as shown in Figure 6a. The extracted pressure driven flow kinetic parameters are compared to the average results of EKF results in rows 1 and 2 of Table 3.

A classical kinetics experiment with varying analyte concentrations of 50, 25, 12.5, 6.25, 3.125, 1.5625, and 0.78 nM has been performed as an additional comparison to the EKF results. The sensorgrams and fits are shown in Figure 6b. The measured response in this case is ∼3 × less than the EKF responses because the maximum concentration of antihuman IgG ∼2.7× less than the EKF experiments. The conventional kinetics results are shown in third row of Table 3. The kinetic parameters and affinity are generally in the same order of magnitude, despite the varying experimental conditions of these experiments, such as pressure driven flow, higher flow rate (120 μL/s), and sample mixing (back and forth motion with 2 μL/s speed using a 100 μL volume) in the flow-cell.

Since high conductivity buffers, such as phosphate buffered saline (PBS), are typically used for hybridization of complex interactant pairs, more investigation is required to minimize the degradation effects of the metal layer. This problem can be solved by coating the gold with a thin silicon-dioxide layer deposited by chemical vapor deposition[51,52] (results not shown). Research is ongoing in our laboratory to implement these improvements and extend the designs from single interactant pairs to multiple interaction measurements. Multiplexing will lead to multiple simultaneous interactions, which do not require any regeneration steps. The large interaction chamber can also be changed to individual microchannels in which the biomolecular interactions are performed, which also does not require any regeneration steps and should be useful for one-shot kinetic analysis.[14]

CONCLUSION

An all electrical electrokinetic sample transport chip has been successfully coupled to an SPR imaging system. Coupled EKF and SPR imaging was successfully demonstrated with a 3% glycerol sample as well as biomolecular interaction of the well-known interactant pairs: human IgG and goat antihuman IgG. The kinetics and affinity parameters extracted from the sensorgrams have been compared to experiments using conventional pressure driven flow and are in good agreement. The distribution of the responses from individual ROIs in the same row was similar for EKF-SPR and conventional pressure driven flow SPR indicating that this approach is viable and does not affect SPR measurements. This successful demonstration of an electrically controlled sample transport system directly coupled to SPR imaging may be important for SPR miniaturization and for scaling systems to accept larger numbers of different samples.

ACKNOWLEDGMENT

The authors thank the Dutch Technology Foundation STW for financial support of the project titled "Multi-analyte food screening with microfluidic biochips". The authors thank Stefan Schlautmann, Hans de Boer, Johan Bomer and Daniel Wijnperlé for their extensive technical support, and Prof. Vinod Subramanian, of the Biophysical Engineering Group of the University of Twente, for general support during the start of the project.

Received for review November 14, 2008. Accepted December 20, 2008.

AC802668Z

(50) Huang, B.; Wu, H.; Kim, S.; Zare, R. N. *Lab Chip* **2005**, *5*, 1005–1007.

(51) Szunerits, S.; Boukherroub, R. *Electrochem. Commun.* **2006**, *8*, 439–444.

(52) Manesse, M.; Stambouli, V.; Boukherroub, R.; Szunerits, S. *Analyst* **2008**, *133*, 1097–1103.